Eur Biophys J (1998) 27: 291–298

ARTICLE

Bruno Gabriel · Justin Teissié

Fluorescence imaging in the millisecond time range of membrane electropermeabilisation of single cells using a rapid ultra-low-light intensifying detection system

Received: 7 August 1997 / Revised version: 14 November 1997 / Accepted: 15 January 1998

Abstract A fast and sensitive fluorescence image acquisition system is described which uses an ultra-low-light intensifying camera able to acquire digitised fluorescence images with a time resolution of 3.33 ms/image. Two modes of recording were employed. The synchronisation mode allowed acquisition of six successive 3.33 ms-images synchronised with an external trigger, while the memorisation mode allowed acquisition of twelve successive 3.33 ms images starting after a 20 ms-time lag from the external trigger. Interaction of ethidium bromide (EB) with the membrane of electropermeabilised living cells was studied using this imaging system. We observed enhanced fluorescence of the dye when associated with electropermeabilised cells. Using single cells, 3.33 ms-images of the fluorescence interaction patterns of ethidium bromide showed well-defined membrane labelling. The enhanced fluorescence patterns were shown to represent the electropermeabilised area of the cell membrane. The average level of fluorescence associated with the labelled part of the cell membrane increased linearly during and immediately (less than 7 ms) after the electropermeabilisation pulse. Steady-state EB interaction with the membrane was achieved in a maximum 20 ms-time lag after electropermeabilisation. The membrane labelled parts were always observed in the cell regions facing the electrodes. They were present only when the electric field strength was higher than a threshold value which was different for the two cell sides. An increase in electric field intensity led to an increase in the dimensions of the labelled cell region.

Key words Millisecond imaging · Fluorescence videomicroscopy · Electropermeabilisation · Electroporation

Part of this work was presented as an oral communication at the 2nd European Biophysics Congress, Orléans, France, July 13–17, 1997.

B. Gabriel (✉) · J. Teissié
Institut de Pharmacologie et de Biologie Structurale-Centre National de la Recherche Scientifique (UPR 9062),
118 Route de Narbonne, F-31062 Toulouse cedex 4, France
(e-mail: gabriel@ipbs.fr)

Abbreviations *EB* Ethidium bromide · *PB* Pulsing buffer · *CHO* Chinese hamster ovary · *ULL* Ultra-low-light · *TTL* Transistor-transistor logic · *LED* Light emitting diode · *CCD* Charge-coupled device

Introduction

Application of brief high-voltage pulses to living cells (electropulsation) makes the cell membrane locally permeable (electropermeabilisation) by significant modulation of the trans-membrane electrical potential difference (Sale and Hamilton 1968; Bernhardt and Pauly 1973). The external electric field locally induces an electrical potential difference ($\Delta\psi_i$) across the cell membrane. Using a physical model describing the living cell as a thin weakly conductive shell (the membrane) full of an internal conductive medium (the cytoplasm), and placed in an external conductive medium, $\Delta\psi_i$ is given by Laplace's equation:

$$\Delta\psi_i\,(M, E, t) = f\, g(\lambda)\, r\, E \cos[\theta(M)]\,(1 - e^{-(t/\tau_m)}) \qquad (1)$$

where M is the point on the cell surface we are considering, t is the time lag after electropulsation is turned on, f is a factor incorporating the spherical geometry of the cell, r is the radius of the pulsed cell, θ (M) is the angle between the direction of the field and the normal of the membrane, E is the external electric field stregth, τ_m is the characteristic time constant of the membrane charging (in the microsecond time range) (Kinosita and Tsong 1977; Ehrenberg et al. 1987), and g(λ) is a parameter controlled by electric conductivities (Gross 1988; Neumann 1989). The biological relevance of this physical description has been experimentally demonstrated on single cells by use of potential sensitive dyes (Gross et al. 1986; Kinosita et al. 1988).

When living cells are electropulsed, the electro-induced potential difference ($\Delta\psi_i$) adds to the resting potential difference ($\Delta\psi_n$). When the new trans-membrane potential difference ($|\Delta\psi_i + \Delta\psi_n|$) locally reaches a critical value, a reversible alteration of the membrane structure leads to membrane permeabilisation (Marszalek et al. 1990; Teissié and

Rols 1993; Gabriel and Teissié 1997). The resting transmembrane potential difference of a living cell is responsible for an asymmetrical electropermeabilisation process (Tekle et al. 1990; Teissié and Rols 1993). Regions of the cell membrane which face the electrodes are permeabilised preferentially (Rossignol et al. 1983; Mehrle et al. 1985; Tekle et al. 1991, 1994; Djuzenova et al. 1996; Gabriel and Teissié 1997). The physical and structural basis of this phenomenon is not yet clear.

The pulse-induced local charging of the membrane is in the microsecond time range (Kinosita and Tsong 1977; Kinosita et al. 1988) and the time courses for the electropermeabilisation of sea urchin eggs were shown to be in the time range 0.5 μs to 1 ms (Hibino et al. 1993). However, other field-induced cell events such as gene transfer require longer electrical pulses (Eynard et al. 1997). Thus, analysis of electropermeabilisation processes requires high temporal and spatial resolution. Observation of transport using single cell video-microscopy, was performed with 17-ms time resolution (Dimitrov and Sowers 1990). Millisecond measurements of the electropermeabilisation-induced transport were obtained by a photometric approach using a single calcein-pre-loaded ghost, but no data were supplied about any preferential transport through electropermeabilised membrane parts (Prausnitz et al. 1995). We have developed a rapid (3.33 ms/image) and ultra-low-light intensifying fluorescence video-microscopy system which we have used to study the electropermeabilisation event of a mammalian cell line, temporally and spatially.

Materials and methods

Chemicals

Ethidium bromide (EB, MW 394.3) was purchased from Sigma. Standard iso-osmotic (312 ± 3 mOs/kg, Osmomat 030 cryoscopic osmometer, Gonotec, Berlin, Germany) pulsing buffer (PB) was 250 mM sucrose, 1 mM $MgCl_2$, and 10 mM potassium phosphate (pH 7.4). The conductivity of PB was 1.5 mS/cm at 21 °C (HI 8820 N conductivity meter, Hanna instruments, Lingolsheim, France).

Cell culture

Chinese hamster ovary (CHO) cells adapted for suspension culture were used to avoid trypsin treatment when cells were collected. They were grown in suspension in completed Eagle's minimum medium MEM 0111 (Eurobio, Les Ulis, France) as previously described (Gabriel and Teissié, 1995a).

Electropulsation of cells

Cells were collected by centrifugation for 10 min at 100 g, washed with PB, and resuspended in 1 mM EB containing PB (10^6 cells/ml). The electropulsation chamber was designed using two stainless steel parallel rods (diameter 0.5 mm, length 10 mm) stuck in a 22 mm × 32 mm glass microscope coverslip. The inter-electrode distance was 5 mm to give a homogeneous uniform electric field. The chamber was placed on the stage of an inverted digitised videomicroscope (Leitz). 70 μl of cell suspension was located between the electrodes and 2 min were allowed for cell sedimentation on the coverslip surface. A single cell with a radius of 6.5 μm was selected by direct measurement in the monitor. A single square-wave unipolar electric pulse with the desired parameters (voltage and duration) was supplied by a CNRS electropulser (Jouan, St. Herblain, France). The rising time of the pulse was 50 ns, and its duration could be selected between 5 μs and 24 ms. Pulse shape was monitored by a 15 MHz oscilloscope (Enertec, St. Etienne, France). Recording of fluorescence images of the electropulsed cell was synchronised with the onset of the electric pulse (synchronisation mode) or was obtained after a maximum 20 ms-time lag from the end of the electric pulse (memorisation mode). Transistor-Transistor Logic (TTL) signals were used for communication between the electropulser and the camera.

Fluorescence image acquisition and processing

The general layout of the ultra-rapid fluorescence image acquisition systems is given in Fig. 1. A single cell in the electropulsation chamber was observed with a Leitz 63 × 1.4 NA oil immersion objective. While the depth of field for this objective was about 1–2 μm, the fluorescence observed in the plane of focus was representative of a 15–20 μm thickness owing to the out-of-focus light contribution (Agard et al. 1989). The inverted microscope was equipped with a HBO 100 W2 lamp (Osram) as excitation light source. The wavelengths were selected using the Leitz N2 filter block (530 nm ≤ λ_{ex} ≤ 560 nm; 580 nm ≤ λ_{em}). The video monitoring set-up was connected to the microscope: the LH 750-ULL rapid camera (Lhesa, Cergy-Pontoise, France) was associated with a Trinitron monitor (Sony, Fellbach, Germany). The camera is an ultra high cadence intensified charge-coupled device (CCD) model which allows real-time fluorescence acquisition at various frequencies (50, 100, 150, 200, 300, and 400 Hz). The image intensifier tube (SuperGen®, Philips) was a double proximity focused (i.e. without electrostatic or electromagnetic lens), 18 mm tube with a S25 photocathode, a glass input, and a P46 phosphor screen. Connection between the image intensifier tube and the CCD image sensor was achieved using a tapering 18/11 mm fiber optic directly fitted to the CCD chip. The interline-type CCD image sensor (ICX024AL-3, Sony) holds a silicon chip with interline transfer. It has a very high sensitivity (2×10^{-5} lux under white light), and a low noise/signal ratio (32 db for 10^{-2} lux). The image size was 8.8 mm (H) × 6.6 mm(V), and the effective pixels were 756 (H) × 581 (V). The unit cell size was 11.0 μm (H) × 11.0 μm (V). Gating was obtained by the electronic shutter of the CCD sensor which brought the best light transfer yield. The gain

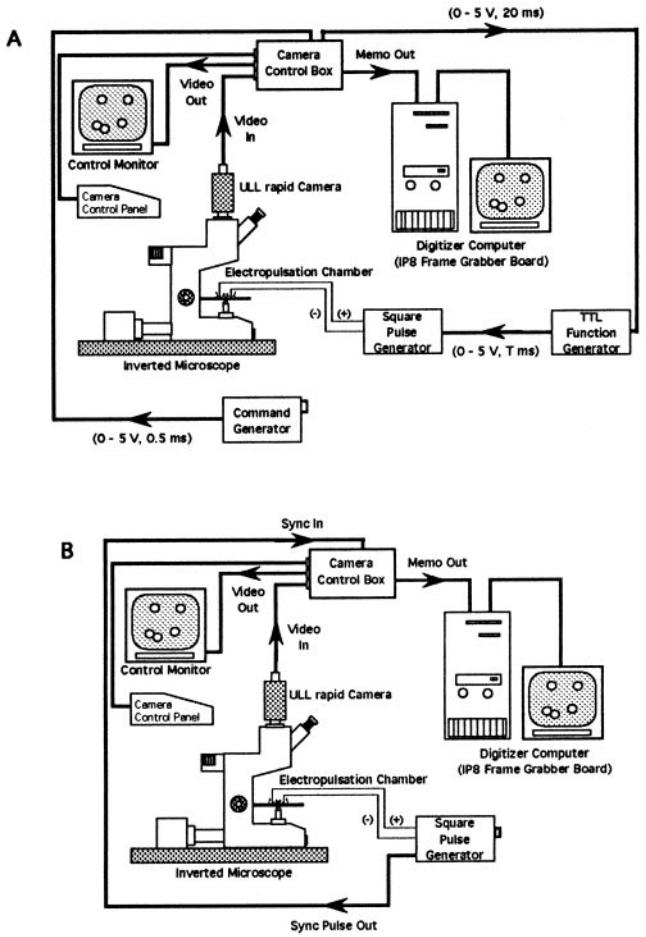

Fig. 1 A, B Schematic drawing of the rapid ultra-low-light intensifying video-microscope system and electropermeabilisation apparatus: **A** Synchronisation mode, **B** Memorisation mode. *Arrows* represent signal directions (TTL and video)

of the camera can be adjusted manually. Using a Leitz 63× 1.4 NA oil immersion objective, the spatial resolution per pixel was 0.2×0.3 μm. Increased image acquisition was obtained by decreasing the area of the camera target scanned. To allow observation of the complete cell we used the 300 Hz acquisition frequency (i.e. 3.33 ms/image). The size of each 3.33 ms image was 512×60. The fluorescence image of the dye was recorded in the memory board of the camera control box. Two modes were used for this work:

a) The synchronisation mode (Fig. 1 A) allowed the acquisition of a single video frame which represented 6 consecutive 3.33 ms-images. The acquisition was synchronised with the onset of the electric pulse by a TTL signal. The falling edge of the TTL signal (1–0, 0.5 ms) generated by the command generator triggered the memorisation of one video frame. The associated TTL signal (0–1, 20 ms) triggered pulsation of cells. As the duration of this TTL signal was constant (20 ms), it was used to trigger a TTL signal, from a function generator which determined the duration of the pulse delivered by the electropulser (0–1, T ms). Owing to the electronic logic of the camera, there was a 3 ms-time lag between the beginning of image acquisition by the camera and the application of the electric field on the cells (Fig. 2 A). This time lag was the first recorded image. This image was therefore considered as the blank image i.e. the fluorescence image of the selected cell before pulsation.

b) The memorisation mode (Fig. 1 B) allowed the acquisition of 2 simultaneous 20 ms video frames, i.e. 12 consecutive 3.33 ms-images. The rising edge of the TTL signal (0–1, T ms) associated with the electric pulse triggered the memorisation of the images by the camera. In this case, the recording of the cell fluorescence pattern began less than 20 ms after the end of the pulse and was randomly distributed between 0 and 20 ms.

The recorded digitised images (8 bits i.e. 256 grey levels) were transferred to a PC computer (AT/486) by using

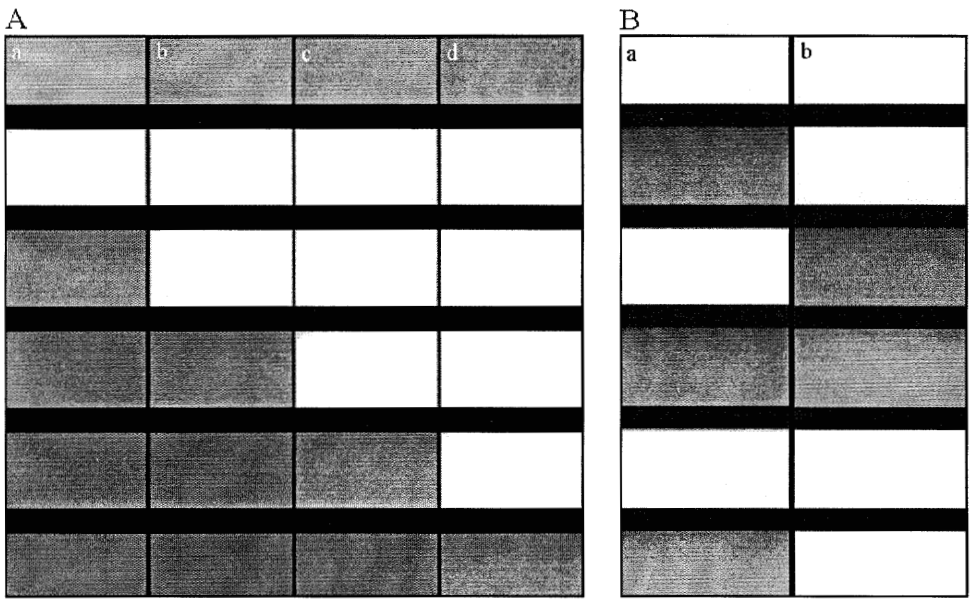

Fig. 2 A, B Validation of the acquisition time resolution of the camera by observation of LED illumination. Single shot observations were used. **A** Validation of the synchronisation mode: *a* one 3.33 ms-pulse, *b* one 6.66 ms-pulse, *c* one 10 ms- pulse, and *d* one 13.33 ms-pulse were applied respectively. **B** Validation of the memorisation mode: only the first six images recorded during the first 20 ms-video frame are shown. **A** train of 3 ms-pulses was applied with a frequency of 150 Hz, **B** train of 6 ms-pulses was applied with a frequency of 75 Hz

a frame grabber board (IP8, Matrox Electronic System, Quebec, Canada). The size of the digitised image was 512×576. Image processing was performed using the Optimas 4.02 software (Bioscan Incorporated, Edmonds, USA). Images were corrected for the background as previously described (Gabriel and Teissié 1995b). Briefly, the blank image (i.e. the background fluorescence) was subtracted from the fluorescence image of the cell after electropulsation. Mathematical amplification of grey levels could be achieved to improve the fluorescence signal linked with electropulsation. Fluorescence emission of the labelled cell part was quantified by measurement of the mean grey level of the region of interest we had previously selected manually.

We used Paint Shop Pro 3.11 software (JASC Inc., Eden Prairie, USA) to prepare images for printing. Final images were printed on a HP Laserjet 4 printer (Hewlett Packard). We used the printer driver software XLI Bitmap Super-Driver (XLI corporation, Woburn, USA) to obtain high resolution halftone prints (2 400 dpi).

Results

Validation of the 750-ULL rapid camera

The acquisition time resolution of the camera was validated by observation, using a 4× objective (Leitz), of a red light emitting diode (LED) switched on for various durations and at different frequencies (Fig. 2). The video system was validated for the two recording modes we developed. Figure 2A shows images obtained with the synchronisation mode. Four pulse durations were used (3, 6, 10, and 13 ms). Only images which were acquired during pulse application showed illumination (white images in Fig. 2A), the other ones represent the background (grey images). Only one 3.33 ms-image showed illumination when one 3 ms-pulse was applied (Fig. 2A-a), while the number of white images increased to two for one 6 ms-pulse (Fig. 2A-b), three for one 10-ms pulse (Fig. 2A-c), and four when a 13-ms pulse was used (Fig. 2A-d). These observations clearly confirmed the occurrence of a time lag of about 3 ms between the onset of the image memorisation and the triggering of the pulse (Fig. 2A). In all experiments, the first image was never illuminated.

Figure 2B shows images obtained with the memorisation mode. Twelve consecutive images were memorised but only the six images recorded during the first 20 ms-video frame are given. We selected recorded images in which the frequencies of memorisation and of LED illumination were synchronous. When the LED was switched on using a train of 3 ms-duration signals applied with a frequency of 150 Hz (Fig. 2B-a), one 3.33 ms-image showed illumination alternatively with one background image. When signals with a 6 ms-duration were applied with a frequency of 75 Hz (Fig. 2B-b), two successive 3.33 ms-images showed illumination alternatively with two background images.

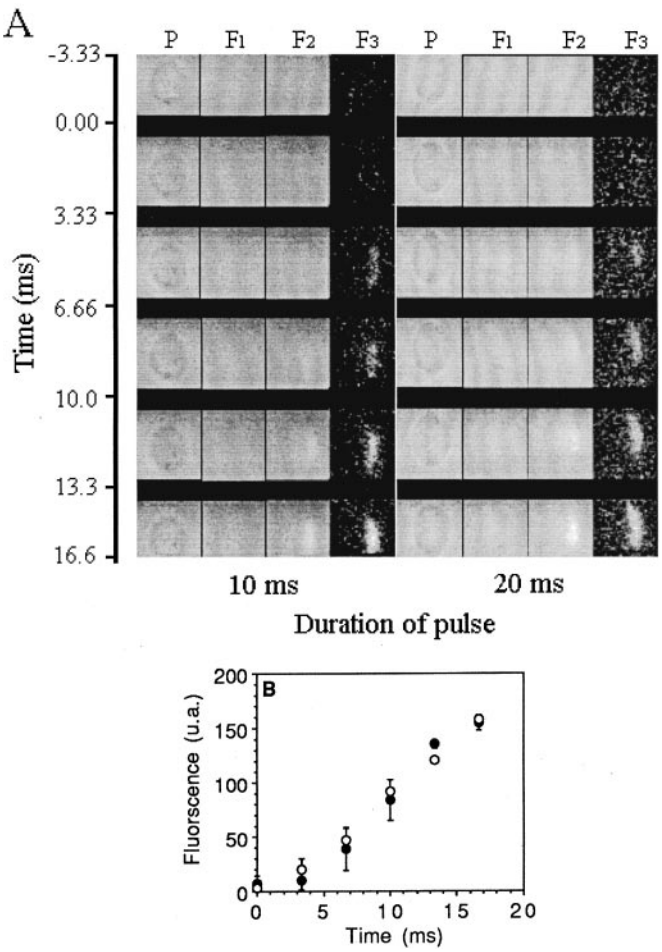

Fig. 3 A, B Time course of EB interaction with the electropermeabilised membrane of a single CHO cell. **A** fluorescence patterns of EB *P* phase-contrast images. *F1* six consecutive raw unprocessed fluorescence images of the CHO cell before pulsation. *F2* consecutive raw unprocessed fluorescence images of the CHO cell obtained synchronously with electropermeabilisation. *F3* mathematically processed images of the CHO cell synchronously obtained to electropermeabilisation (i.e. *F2* images minus *F1* images). Fluorescence levels in *F3* were digitally amplified 3 fold. Cells were electropermeabilised in 1 mM EB-containing PB, using a single pulse of 1.1 kV/cm with 10 and 20 ms duration, respectively. The position of the electrodes is: positive (anode) to the right and negative (cathode) to the left of each image. Image acquisition frequency was 300 Hz (3.33 ms/image). The localised enhanced peripheral fluorescence indicates the EB-associated cell staining. The time scale on the left of the figure, is associated with the *F2* and *F3* images. Zero is indicative of the beginning of the electric pulse. **B** Time course of the electro-induced increase of the fluorescence emission of the labelled part on the electropermeabilised cell. Cells were electropermeabilised in 1 mM EB-containing PB, using a single pulse of 1.1 kV/cm with (○) 10 ms and (●) 20 ms duration

Interaction of the fluorescence dye with the electropermeabilised cell, synchronously with electric field application

Electropermeabilisation of a single CHO cell in suspension was monitored by using EB which is naturally relatively membrane impermeant (Sixou and Teissié 1993). Figure 3A shows the typical sequence of images obtained

before and synchronously with the application of a single pulse of 1.1 kV/cm with different durations (10 and 20 ms) on a CHO cell in 1 mM EB-containing PB. The raw unprocessed images obtained before and synchronously with the electropulsation were reported (Fig. 3A F1–F2). Data analysis make use of the pre-pulse images (F1 in Fig. 3A) as background images substracted from subsequent images (F2 in Fig. 3A). Fluorescence enhancement (F3 in Fig. 3A) was observed as soon as the electric field with a subcritical strength was applied. Interaction of EB with the electropermeabilised cell was visualised by the peripheral area with enhanced fluorescence. The shape and the localisation of this fluorescence pattern appeared to be characteristic of membrane or very near-membrane labelling (El Ouagari et al. 1993) and was not due to the binding of EB to the nuclear DNA (Gabriel and Teissié, 1997), which typically occurred only over a period of 2–5 minutes. The fluorescence areas were always facing the anode electrode. Peripheral labelling present on the anode-facing side of the electropulsed cell only occurred when the cell was pulsed with electric field strengths higher than about 500 V/cm (data not shown). The average grey levels of the fluorescence regions were measured and the kinetics of their in- and post-pulsation increases were reported when a single 1.1-kV/cm pulse was applied (Fig. 3B). The same kinetics were obtained when one 10-ms pulse and one 20-ms pulse were applied to the cell. The fluorescence level increased linearly when the electric field was applied, and the slope of the fluorescence increase did not depend on the duration of the pulse.

Post-pulsation interaction of the fluorescence dye with the electropermeabilised cell

Using the memorisation mode, the interaction of EB with an electropermeabilised cell observed about 20-ms after pulsation, gave limited areas on the cell periphery with enhanced fluorescence (Figs. 4A and B). When a single 20 ms-electric pulse with an intensity of 600 V/cm was applied, one peripheral fluorescence area was observed facing the positive electrode (anode) (Fig. 4A). When the electric field strength was 1100 V/cm, two opposite peripheral fluorescence areas were observed and they both faced the electrodes (Fig. 4B). It was therefore possible to measure graphically the angles θ_a and θ_c defined as half of

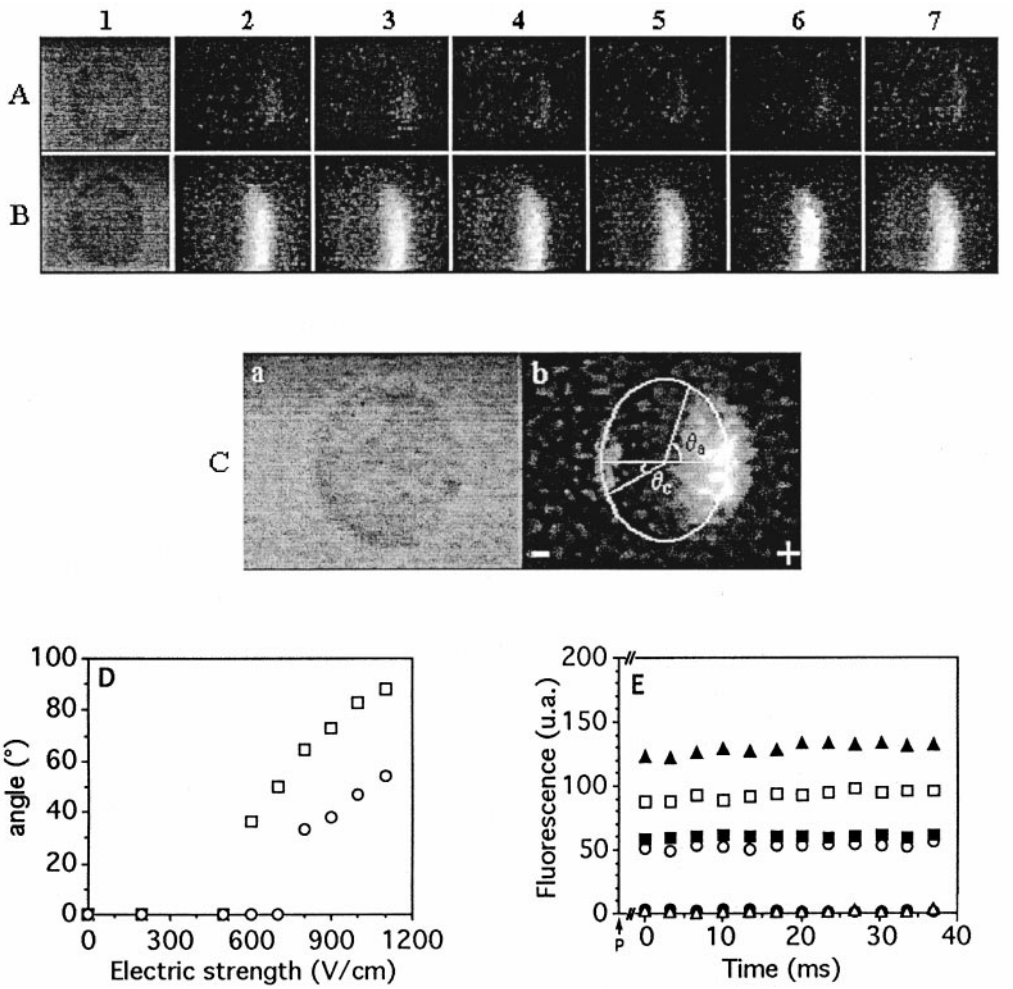

Fig. 4A–E Post-pulsation interaction of EB with the electropermeabilised CHO cell: electropermeabilisation was achieved in 1 mM EB-containing PB using a single 20 ms-pulse. The position of the electrode is as shown: positive (anode) to the right and negative (cathode) to the left of each image. **A** images showing the fluorescence patterns of EB associated with a single electropermeabilised CHO cell using 600 V/cm. *1* phase-contrast image of the cell before electropulsation, *2–7* first six 3.33 ms-images from the twelve recorded. **B** images showing the fluorescence patterns of EB associated with a single electropermeabilised CHO cell using 1100 V/cm. *1* phase-contrast image of the cell before electropulsation, *2–7* first six 3.33 ms-images from the twelve recorded. **C** determination of the experimental polar angle: *a* phase-contrast of the cell, *b* EB fluorescence mode, after electropermeabilisation using one 20 ms-pulse of 800 V/m. Fluorescence levels were digitally amplified 3 fold. **D** dependence of the polar angle in the electric field strength: □ angle facing the anode θ_a, ○ angle facing the cathode θ_c. **E** time dependence of the fluorescence emission in a maximum 20-ms time lag after electropulsation. Electric field intensities were △ 0 V/cm, ● 500 V/cm, ○ 600 V/cm, ■ 700 V/cm, □ 800 V/cm, and ▲ 900 V/cm. P (arrow) is indicative of the electropulsation

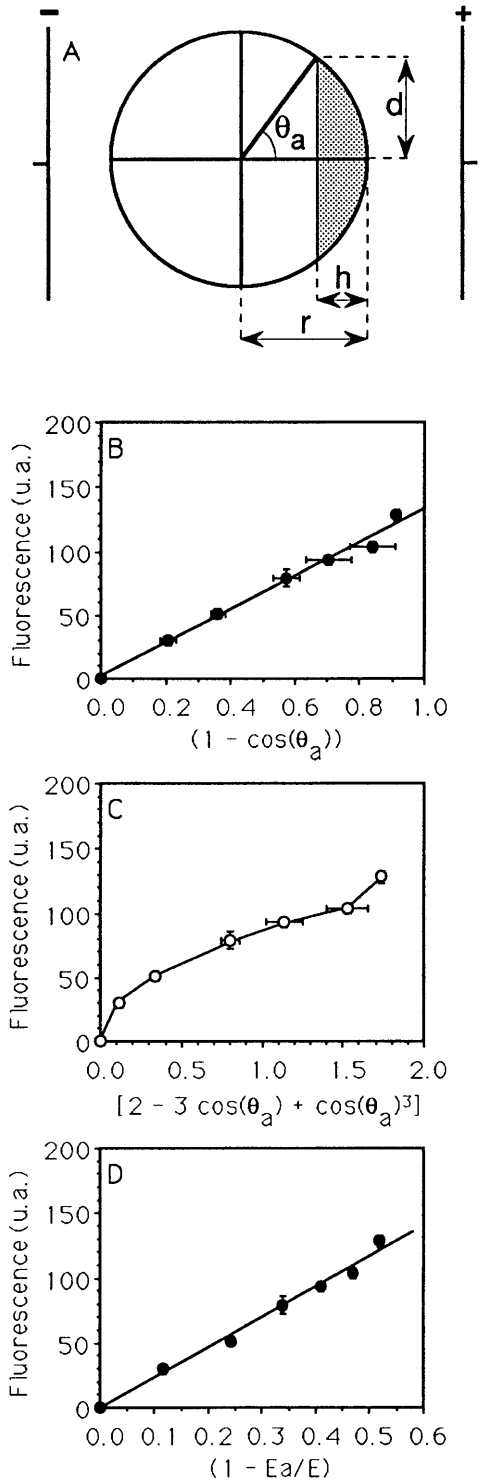

Fig. 5 A–D Localisation of the labelled part on an electropermeabilised CHO cell: electropermeabilisation was achieved in 1 mM EB containing PB using a single 20 ms-pulse. **A** schematic drawing of the anode-facing fluorescence pattern and associated parameters, **B** dependence of the EB fluorescence emission on the membrane surface limited by the angle θ_a, correlation coefficient of the linear fit was found to be 0.97. **C** dependence of the EB fluorescence emission on the cell cap volume limited by the angle θ_a, **D** relation between the extent of membrane area electrically altered and the EB fluorescence emission after pulsation. Fluorescence levels were reported as a function of $(1-E_a/E)$, with E_a equal to 530 V/cm. Correlation coefficient of the linear fit was found to be 0.98

the polar angle of the fluorescence part present on the anode- and cathode-facing sides of the cell respectively (Fig. 4C). Peripheral labelling present on the anode-facing side of the electropulsed cell only occurred when the cell was pulsed with electric field strengths higher than about 500 V/cm. Peripheral labelling present on the cathode-facing side of the electropulsed cell only occurred when the cell was pulsed with electric field strengths higher than about 750 V/cm (data not shown). Above these threshold values, any increase in electric field intensity led to an increase in the size of the labelled cell parts (Fig. 4D), and therefore in the average fluorescence levels (Fig. 4E). However, for a given electric field strength, the average fluorescence level of the labelled area remained constant right through the total time of observation (40 ms; i.e. 12 successive images) (Fig. 4E).

Localisation of the labelled part of electropermeabilised cell

Figure 5A is a schematic drawing showing the anode-facing fluorescence pattern observed when the cell has been electropermeabilised. The dimensions of this labelled part were measured using the following two parameters:

$$h = r\,(1-\cos\theta_a) \tag{2}$$

and,

$$d = r \sin\theta_a\,. \tag{3}$$

The surface S_m of the cell membrane which is limited by the angle θ_a associated with the labelled region is:

$$S_m = 2\,\pi\,r\,h = 2\,\pi\,r^2\,(1-\cos\theta_a)\,. \tag{4}$$

Figure 5B shows the dependence of the average fluorescence of the labelled cell part on the surface parameter $(1-\cos\theta_a)$ in Eq. (4). While the illumination of the cell is not truly homogeneous, the enhanced fluorescence of the dye was linearly related to the surface of the cell membrane defined by the angle θ_a.

The volume V_c of the cell cap included in the labelled region limited by the angle θ_a is:

$$V_c = \pi\,(r\,h^2 - h^3/3) = \pi\,[2 - 3\cos\theta_a + (\cos\theta_a)^3]\,r^3/3\,. \tag{5}$$

Figure 5C shows the dependence of the average fluorescence level of the labelled cell part on the cap volume, i.e. $[2 - 3\cos\theta_a + (\cos\theta_a)^3]$ in Eq. (5). No statistically relevant linear fit could be found between the enhanced fluorescence of EB and the volume of the cell cap.

The fluorescence level associated with the labelled cell region depended on the electric field strength (Fig. 4E). The dependence of the fluorescence on the electric field intensity was reported as a function of $(1 - E_a/E)$ in which E_a was the threshold electric field strength value which triggered membrane electropermeabilisation on the anode-facing side of the cell. E_a was graphically found to be

530 ± 38 V/cm from the linear dependence of θ_a on the reciprocal of the field strength (data not shown) (Gabriel and Teissié 1997). $(1 - E_a/E)$ represents the extent of permeabilised membrane area (Schwister and Deutike 1985; Rols and Teissié 1990). Results show a linear relationship between fluorescence level and electropermeabilised membrane area. This supports our previous conclusions that the electropermeabilisation is homogeneous over this area, at a given field strength and pulse duration (Rols and Teissié 1990; Gabriel and Teissié 1997).

Similar behaviour of the fluorescence dependence was obtained regarding the cathode-facing cell hemisphere (data not shown). The threshold electric field strength value which triggered membrane electropermeabilisation on the cathode-facing cell side was found to be 730 ± 80 V/cm.

Discussion

We have developed a rapid ultra-low-light intensifying video-microscope system. Two modes of image recording, both triggered by an external signal, are described (Fig. 1). They allowed fluorescence image acquisition on a single cell with a very short time resolution (3.33 ms/image). The synchronisation mode allowed acquisition of six successive 3.33 ms-images in synchronisation with the external trigger. In this configuration, the first image represented the fluorescence background and the next five images were representative of the events occurring when the trigger signal was applied (Fig. 2A). The synchronisation mode could be used to observe biological events triggered synchronously with an external short stimulus (e.g. caged-compound release after light flash, electro-induced molecular transport across a cell membrane, etc.). We used it to follow the interaction of an external dye (EB) with the electropermeabilised parts of a single CHO cell during the application of the electropermeabilisation pulse (Fig. 3A). This system allowed us to observe on a single cell, and during the application of the external electric pulse, a time-varying molecular event directly associated with the membrane electropermeabilisation. Analysis of the time course of EB-associated membrane staining (Fig. 3B) showed that the rate of the process is not dependent on the pulse duration. Furthermore when one 10 ms-pulse was applied, the increase of fluorescence was still observed immediately after the pulse application. These observations are opposite to what one would expect for the involvement of electrophoresis or electroosmosis transport during the pulse, as proposed by others (Dimitrov and Sowers 1990; Prausnitz et al. 1995).

The memorisation mode allowed acquisition of twelve successive 3.33 ms-image in a maximum 20-ms time lag after the end of the trigger signal. This mode could be used to observe remnant events immediately after the application of an external stimulus. The acquisition time resolutions of the two recording systems were validated by observation of LED illumination with different durations and frequencies (Fig. 2). Then, we analysed biological events on single electropermeabilised CHO cells.

EB is classically known as a nucleic acid stain. Its fluorescence properties specifically allow the observation of its entry into electropermeabilised cells (Sixou and Teissié 1993; Tekle et al. 1994; Gabriel and Teissié 1997). On the other hand, it has previously been described as a tool for the study of biological membranes owing to its change in emission when bound to membrane loci (Gitler et al. 1969). Fluorescence spectra and the quantum yield of EB are highly environment-dependent and the increase in fluorescence of EB when interacting with the electropermeabilised cell membrane reflects the immersion of the dye in a more structured and/or hydrophobic environment. Using EB and the rapid ultra-low-light intensifying acquisition system, we visualise peripheral fluorescence regions associated with the electropermeabilised state of CHO cells. A slow trans-membrane inflow of the dye takes place and is associated with the electropermeabilised state of the membrane (Sixou and Teissié 1993; Tekle et al. 1994; Gabriel and Teissié 1997). A continuous increase of the dye emission would be expected if fluorescence was associated with intracellular binding of EB to its classical targets (i.e. RNAs and nuclear DNA). Kinetic analysis of the fluorescence emission of the labelled cell parts showed that there was no detectable change within 40 ms (Fig. 4A, B and E). This stable and fast labelling appears to depict the steady state of EB interaction with the electropermeabilised cell membrane. Enhanced EB fluorescence should be due to a direct interaction of the dye with the membrane compounds (Gitler et al. 1969) rather than to binding of the dye to cytoplasmic targets localised close to the membrane. Furthermore, a linear relationship was only found between the fluorescence emission of EB and the surface of the labelled cell cap (Fig. 5B). Our system therefore allowed clear determination of the membrane area with which EB interacted. Experimental characteristic angles could be obtained graphically (Fig. 3C). Our observations agree with the theory of asymmetric electropermeabilisation (Tekle et al. 1990; Teissié and Rols 1993; Gabriel and Teissié 1997).

The dimension of the labelled membrane region depended on the reciprocal of the applied electric field strength (Fig. 4D). Figure 5D shows that the average fluorescence level of the labelled cell membrane part depends linearly on the surface of the electropermeabilised membrane part. The linear fit obtained indicated that the interaction of the dye with the membrane was only present on the electropermeabilised part of the cell surface. The part of the cell membrane globally affected by the electrical treatment depended on the applied electric field strength as previously reported (Schwister and Deutike 1985; Rols and Teissié 1990; Gabriel and Teissié 1997).

Study of the electropermeabilisation-induced membrane events using the synchronisation mode is currently under investigation in our laboratory.

Acknowledgements Thanks are due to Mr Ph. Vallois (Lhesa electronique) for providing technical information, to Ms M. Golzio for her comments, and to Mr J. Robb for reading the manuscript. This work was partly supported by funds from the Association pour la Recherche contre le Cancer, and from the Ministère de l'Education

Supérieure et de la Recherche ACR “Physicochimie des membranes biologiques”.

References

Agard DA, Hiraoka Y, Shaw P, Sedat JW (1989) Fluorescence microscopy in three dimensions. Methods Cell Biol 30: 353–377

Bernhardt J, Pauly H (1973) On the generation of potential difference across the membrane of ellipsoidal cells in an alternating electric field. Biophysik 10: 89–98

Dimitrov DS, Sowers AE (1990) Membrane electroporation-fast molecular exchange by electroosmosis. Biochim Biophys Acta 1022: 381–392

Djuzenova CS, Zimmermann U, Frank H, Sukhorukov VL, Richter E, Fuhr G (1996) Effect of medium conductivity and composition on the uptake of propidium iodide into electropermeabilized myeloma cells. Biochim Biophys Acta 1284: 143–152

Ehrenberg B, Farkas DL, Fluhler EN, Lojewska Z, Loew LM (1987) Membrane potential induced by external electric field pulses can be followed with a potentiometric dye. Biophys J 51: 833–837

El Ouagari K, Gabriel B, Benoist H, Teissié J (1993) Electric field-mediated glycophorin insertion in cell membrane is a localized event. Biochim Biophys Acta 1151: 105–109

Eynard N, Rols MP, Ganeva V, Galutzov B, Sabri N, Teissié J (1997) Electrotransformation pathways of procaryotic and eucaryotic cells. Recent developments. Bioelectrochem Bioenerg 44: 103–110

Gabriel B, Teissié J (1995 a) Control by electrical parameters of short- and long-term cell death resulting from electropermeabilization of Chinese hamster ovary cells. Biochim Biophys Acta 1266: 171–178

Gabriel B, Teissié J (1995 b) Spatial compartmentation and time resolution of photooxidation of a cell membrane probe in electropermeabilized Chinese hamster ovary cells. Eur J Biochem 228: 710–718

Gabriel B, Teissié J (1997) Direct observation in the millisecond time range of fluorescent molecule asymmetric interaction with the electropermeabilized cell membrane. Biophys J 73: 2630–2637

Gitler C, Rubalcava B, Caswell A (1969) Fluorescence changes of ethidium bromide on binding to erythrocyte and mitochondrial membranes. Biochim Biophys Acta 193: 479–481

Gross D, Loew LM, Webb WW (1986) Optical imaging of cell membrane potential changes induced by applied electric fields. Biophys J 50: 339–348

Gross D (1988) Electromobile surface charge alters membrane potential changes induced by applied electric fields. Biophys J 54: 879–884

Hibino M, Itoh H, Kinosita KJr (1993) Time courses of cell electroporation as revealed by submicrosecond imaging of transmembrane potential. Biophys J 64: 1789–1800

Kinosita KJr, Tsong TY (1977) Voltage induced pore formation and hemolysis of human erythrocytes. Biochim Biophys Acta 471: 227–242

Kinosita KJr, Ashikawa I, Saita N, Yoshimura H, Itoh H, Nagayama K, Ikegami A (1988) Electroporation of cell membrane visualized under a pulsed-laser fluorescence microscope. Biophys J 53: 1015–1019

Marszalek P, Liu DS, Tsong TY (1990) Schwan equation and transmembrane potential induced by alternating electric field. Biophys J 58: 1053–1058

Mehrle W, Zimmermann U, Hampp R (1985) Evidence for asymmetrical uptake of fluorescent dyes through electro-permeabilized membrane of *Avena* mesophyll protoplast. FEBS Lett 185: 89–94

Neumann E (1989) The relaxation hysteresis of membrane electroporation. In: Neumann E, Sowers AE, Jordan Ca (eds) Electroporation and Electrofusion in Cell Biology. Plenum Press, New York, pp 61–82

Prausnitz MR, Corbett JD, Gimm JA, Golan DE, Langer R, Weaver JC (1995) Millisecond measurement of transport during and after an electroporation pulse. Biophys J 68: 1864–1870

Rols MP, Teissié J (1990) Electropermeabilization of mammalian cells. Quantitative analysis of the phenomenon. Biophys J 598: 1089–1098

Rossignol DP, Decker GL, Lennarz WJ, Tsong TY, Teissié J (1983) Induction of calcium-dependent, localized cortical granule breakdown in sea-urchin eggs by voltage pulsation. Biochim Biophys Acta 763: 346–355

Sale JH, Hamilton WA (1968) Effects of high electric field in microorganisms. III. Lysis of erythrocytes and protoplasts. Biochim Biophys Acta 163: 37–43

Schwister K, Deuticke B (1985) Formation and properties of aqueous leaks induced in human erythrocytes by electrical breakdown. Biochim Biophys Acta 816: 332–348

Sixou S, Teissié J (1993) Exogenous uptake and release of molecules by electroloaded cells: a digitized videomicroscopy study. Bioelectrochem Bioenerg 31: 237–257

Teissié J, Tsong TY (1981) Electric field induced transient pores in phospholipid bilayer vesicles. Biochemistry 20: 1548–1554

Teissié J, Rols MP (1993) An experimental evaluation of the critical potential difference inducing cell membrane electropermeabilization. Biophys J 65: 409–413

Tekle E, Astumian RD, Chock PB (1990) Electro-permeabilization of cell membrane: Effect of the resting membrane potential. Biochem Biophys Res Commun 172: 282–287

Tekle E, Astumian RD, Chock PB (1991) Electroporation by using bipolar oscillating electric field: An improved method for DNA transfection of NIH 3T3 cells. Proc Natl Acad Sci USA 88: 4230–4234

Tekle E, Astumian RD, Chock PB (1994) Selective and asymmetric molecular transport across electroporated cell membranes. Proc Natl Acad Sci USA 91: 11512–11516